Use of Model-Based Parameter Estimation for Fast RCS Computation of a Conducting Body of Revolution over a Frequency Band

Hyunwung Son, Joseph R. Mautz, and Ercument Arvas
Department of Electrical Engineering and Computer Science
Syracuse University, Syracuse, NY 13244
hson@syr.edu, jrmautz@syr.edu, earvas@syr.edu

***Abstract*—Frequency-derivative information incorporated with model-based parameter estimation (MBPE) is used to obtain scattering from a perfectly conducting body of revolution (BOR). The electric field integral equation (EFIE) is solved using the method of moments (MoM) to obtain the surface current on the perfectly conducting body. Instead of computing the MoM solution using a pointwise approach, a rational function model is used to approximate the current as a function of frequency. The model coefficients are computed using both frequency and frequency-derivative information at one frequency in the band or alternatively two or more frequencies in the band. With the rotational symmetry of BOR, the computational cost can be significantly reduced compared to that of arbitrary three-dimensional (3-D) objects and more importantly scattering from an electrically large body can be obtained. Numerical results for various perfectly conducting bodies are presented. Results show that the MBPE provides excellent agreement with the pointwise approach over a limited frequency band. In addition, the MBPE performs well for predicting sharp resonances.**

I. INTRODUCTION

Most electromagnetic problems are essentially involved in determining the response over a certain bandwidth rather than at one or a few sampling points. Traditionally when the solution over a frequency band is required, a conventional method such as the method of moments (MoM) uses a set of discrete frequency samples with linear or low order polynomial interpolation, which requires a large number of frequency samples to obtain an accurate frequency response curve over the frequency band. In addition, for a response which contains very sharp resonances or is high Q, an excessive number of closely spaced frequency samples are required. As a result, the computational cost would be very high.

In [1]–[2], model-based parameter estimation (MBPE) is introduced to obtain a frequency response curve from both frequency and frequency-derivative data in a procedure where the moment matrix equation is differentiated. As an application, MBPE is used to evaluate the specialized Green's function associated with scatterers inside rectangular guided-wave structures and cavities [3]. Typically, MBPE is applied to predict the radar scattering cross section (RCS) of conducting and dielectric two-dimensional (2-D) bodies over a frequency band [4], [5] and of arbitrarily shaped three-dimensional (3-D) perfectly electric conducting (PEC) objects versus frequency [6], [7]. Specifically, in [4]–[7], the current is approximated by a rational function and its coefficients are determined using frequency and frequency-derivative data. In addition to a one-frequency derivative method, a multi-frequency derivative method has been presented [4], [7]. As a similar approach, Cauchy's technique is utilized to determine the electromagnetic response of a conducting cylinder over a frequency band and the coefficients of the rational function are obtained from the current and its derivatives at a few frequency points [8].

In this work, MBPE is applied to evaluate scattering from a conducting body of revolution (BOR) over a certain frequency range. In fact, the problem of electromagnetic scattering from a BOR has been studied by lots of researchers for many years [9]–[15]. With the rotational symmetry of BOR, the original 3-D problem can be reduced to a series of 2-D problems. As a result, electromagnetic scattering from a BOR can be computed with a significant reduction of computational time and data storage. However, when the frequency response over a frequency band is required, computations involving a BOR can be costly when the pointwise approach is used.

In this work, instead of using a pointwise approach, a rational function model is utilized to approximate the current as a function of frequency and the model coefficients are determined using both frequency information and frequency-derivative information within a frequency band. Consequently, the computational cost can be dramatically reduced.

II. MODEL-BASED PARAMETER ESTIMATION

A. Computing model coefficients using frequency-derivative samples

The fundamental spectral-domain rational function model can be written as

$$F(X) = \frac{N(X)}{D(X)} = \frac{\left[\sum_{i=0}^{n} N_i X^i\right]}{\left[\sum_{i=0}^{d} D_i X^i\right]} \tag{1}$$

where X would be the complex frequency ($X = \sigma + j\omega$). Of course, polynomials of any orders can be used in the numerator and denominator of this model. The N_i's and D_i's of (1) can be found when frequency-derivative samples at a certain frequency

are available. To find them, we begin by rewriting (1) as

$$F(X)D(X) = N(X). \tag{2}$$

Starting with (2) and differentiating t times with respect to X, the following results occur

$$\begin{aligned} &F'D + FD' = N' \\ &F''D + 2F'D' + FD'' = N'' \\ &\quad\vdots \\ &F^{(t)}D + tF^{(t-1)}D' + \cdots + \binom{t}{t-m}F^{(m)}D^{(t-m)} \\ &\qquad + \cdots + FD^{(t)} = N^{(t)} \end{aligned} \tag{3}$$

where $\binom{t}{t-m}$ is the binomial coefficient, and X dependance is implicit. Equations (2) and (3) form a system of $t+1$ equations that can be used to determine the model coefficients.

If the frequency derivatives are known at only a single frequency X_0, (2) and (3) can be simplified by replacing X by $X - X_0$ where $X - X_0$ represents the frequency deviation from X_0. Then setting $D_0 = 1$, setting $t = n + d$, and defining $\mathcal{D} = t + 1$, we have the following matrix equation for the unknown coefficients

$$[A]\,[B] = [C] \tag{4}$$

where $A =$

$$\begin{bmatrix} 1 & 0 & \cdots & \cdots & 0 & 0 & 0 & \cdots & 0 \\ 0 & 1 & \cdots & \cdots & 0 & -F_0 & 0 & \cdots & 0 \\ 0 & 0 & 1 & \cdots & 0 & -F_1 & -F_0 & \cdots & 0 \\ \vdots & & & \ddots & \vdots & \vdots & \vdots & \ddots & \vdots \\ 0 & 0 & \cdots & \cdots & 1 & -F_{n-1} & -F_{n-2} & \cdots & -F_{n-d} \\ 0 & 0 & \cdots & \cdots & 0 & -F_n & -F_{n-1} & \cdots & -F_{n-d+1} \\ \vdots & & & \ddots & \vdots & \vdots & \vdots & \ddots & \vdots \\ 0 & 0 & \cdots & \cdots & 0 & -F_{\mathcal{D}-2} & -F_{\mathcal{D}-3} & \cdots & -F_{\mathcal{D}-d-1} \end{bmatrix} \tag{5}$$

$$B = \begin{bmatrix} N_0 & N_1 & N_2 & \cdots & N_n & D_1 & \cdots & D_d \end{bmatrix}^T \tag{6}$$

$$C = \begin{bmatrix} F_0 & F_1 & F_2 & \cdots & F_n & F_{n+1} & \cdots & F_{\mathcal{D}-1} \end{bmatrix}^T \tag{7}$$

where $F_m = (1/m!)F^{(m)}(0)$ for $m = 0, 1, \ldots, \mathcal{D} - 1$ and $F_m = 0$ when $m < 0$, F is regarded as a function of $(X - X_0)$, and the superscript T denotes the transpose of a row vector. By solving (4), we obtain the unknown coefficients.

If the frequency-derivative information is available at more than one frequency, then a more general matrix equation needs to be taken instead of (4). Let us consider a two-frequency model and choose sampling points at two frequencies X_1 and X_2. If we have one frequency sample and n frequency-derivative samples at X_1 and one frequency sample and $d - 1$ frequency-derivative samples at X_2 then the system of $n+d+1$ equations can be solved. In detail, (2) can be expanded as the following equation at the first sampling point X_1

$$\begin{aligned} &N_0 + N_1X_1 + N_2X_1^2 + \cdots + N_nX_1^n \\ &\quad = (1 + D_1X_1 + D_2X_1^2 + \cdots + D_dX_1^d)F(X_1) \\ &\quad = F(X_1) + D_1F(X_1)X_1 + D_2F(X_1)X_1^2 \\ &\qquad + \cdots + D_dF(X_1)X_1^d \end{aligned} \tag{8}$$

Similarly, (2) can be expanded as the following equation at the second sampling point X_2

$$\begin{aligned} &N_0 + N_1X_2 + N_2X_2^2 + \cdots + N_nX_2^n \\ &\quad = (1 + D_1X_2 + D_2X_2^2 + \cdots + D_dX_2^d)F(X_2) \\ &\quad = F(X_2) + D_1F(X_2)X_2 + D_2F(X_2)X_2^2 \\ &\qquad + \cdots + D_dF(X_2)X_2^d \end{aligned} \tag{9}$$

Differentiating (8) n times with respect to X_1 and differentiating (9) $d - 1$ times with respect to X_2, we can obtain the following matrix equation to compute the unknown coefficients,

$$\begin{bmatrix} A_{M_1} & B_{M_1} \\ A_{M_2} & B_{M_2} \end{bmatrix} [C_M] = \begin{bmatrix} D_{M_1} \\ D_{M_2} \end{bmatrix} \tag{10}$$

where

$$A_{M_1} = \begin{bmatrix} 1 & X_1 & X_1^2 & \cdots & X_1^n \\ 0 & 1 & 2X_1 & \cdots & nX_1^{n-1} \\ \vdots & \vdots & \ddots & \vdots & \vdots \\ 0 & 0 & 0 & \cdots & \frac{d^n}{dX_1^n}N(X_1) \end{bmatrix} \tag{11}$$

$$A_{M_2} = \begin{bmatrix} 1 & X_2 & X_2^2 & \cdots & X_2^n \\ 0 & 1 & 2X_2 & \cdots & nX_2^{n-1} \\ \vdots & \vdots & \ddots & \vdots & \vdots \\ 0 & 0 & 0 & \cdots & \frac{d^{d-1}}{dX_2^{d-1}}N(X_2) \end{bmatrix} \tag{12}$$

$$B_{M_1} = \begin{bmatrix} -F(X_1)X_1 & \cdots & -F(X_1)X_1^d \\ -\frac{d}{dX_1}\{F(X_1)X_1\} & \cdots & -\frac{d}{dX_1}\{F(X_1)X_1^d\} \\ \vdots & \vdots & \\ -\frac{d^n}{dX_1^n}\{F(X_1)X_1\} & \cdots & -\frac{d^n}{dX_1^n}\{F(X_1)X_1^d\} \end{bmatrix} \tag{13}$$

$$B_{M_2} = \begin{bmatrix} -F(X_2)X_2 & \cdots & -F(X_2)X_2^d \\ -\frac{d}{dX_2}\{F(X_2)X_2\} & \cdots & -\frac{d}{dX_2}\{F(X_2)X_2^d\} \\ \vdots & \vdots & \\ -\frac{d^{d-1}}{dX_2^{d-1}}\{F(X_2)X_2\} & \cdots & -\frac{d^{d-1}}{dX_2^{d-1}}\{F(X_2)X_2^d\} \end{bmatrix} \tag{14}$$

$$C_M = \begin{bmatrix} N_0 & N_1 & \cdots & N_n & D_1 & D_2 & \cdots & D_d \end{bmatrix}^T \tag{15}$$

$$D_{M_1} = \begin{bmatrix} F(X_1) & \frac{d}{dX_1}F(X_1) & \cdots & \frac{d^n}{dX_1^n}F(X_1) \end{bmatrix}^T \tag{16}$$

$$D_{M_2} = \begin{bmatrix} F(X_2) & \frac{d}{dX_2}F(X_2) & \cdots & \frac{d^{d-1}}{dX_2^{d-1}}F(X_2) \end{bmatrix}^T \tag{17}$$

where the superscript T denotes the transpose of a row vector. By solving (10), we obtain the unknown coefficients.

B. Computing frequency derivatives in a method of moments model

Following the development in [16], one obtains the following moment equation

$$Z\,\vec{I} = \vec{V} \tag{18}$$

$$Z = \begin{bmatrix} Z_n^{tt} & Z_n^{t\phi} \\ Z_n^{\phi t} & Z_n^{\phi\phi} \end{bmatrix} \tag{19}$$

$$\vec{I} = \begin{bmatrix} I_n^{tq} \\ I_n^{\phi q} \end{bmatrix} \tag{20}$$

$$\vec{V} = \begin{bmatrix} V_n^{tq} \\ V_n^{\phi q} \end{bmatrix} \tag{21}$$

where Z, $\vec{I}$, and $\vec{V}$ are the $N \times N$ moment matrix and current and voltage $N \times 1$ column vectors respectively, and they are all functions of frequency through $k = \omega\sqrt{\mu\epsilon}$ where ω is the angular frequency.

In this work, surface currents are modeled by rational functions of frequency. In detail we assume that the i^{th} element of $\vec{I}$ in (18) is $I_i(k)$ modeled by

$$I_i(k) = \frac{N(k)}{D(k)} = \frac{\sum_{j=0}^{n} N_j\, k^j}{\sum_{j=0}^{d} D_j\, k^j} \tag{22}$$

in which there are $n + d + 1$ coefficients (N_j's and D_j's) to be determined (assume that $D_0 = 1$). The N_j's and D_j's of (22) can be found when frequency and frequency-derivative samples at a certain frequency are available.

Starting with (18) and differentiating t times with respect to k, there results the following:

$$\begin{aligned} &Z\vec{I} = \vec{V} \\ &Z'\vec{I} + Z\vec{I}\,' = \vec{V}\,' \\ &Z''\vec{I} + 2Z'\vec{I}\,' + Z\vec{I}\,'' = \vec{V}\,'' \\ &\quad\vdots \\ &Z^{(t)}\vec{I} + tZ^{(t-1)}\vec{I}\,' + \cdots + \binom{t}{t-m} Z^{(m)}\vec{I}^{(t-m)} \\ &\qquad + \cdots + Z\vec{I}^{(t)} = \vec{V}^{(t)} \end{aligned} \tag{23}$$

where $\binom{t}{t-m}$ is the binomial coefficient and the k dependence is implicit. Solving the $(s+1)^{th}$ of matrix equations (23) for $\vec{I}^{(s)}$ in terms of $\vec{I}, \vec{I}^{(1)}, \ldots, \vec{I}^{(s-1)}$, we obtain

$$I_i^{(s)} = \sum_{j=1}^{N} Y_{ij} \left[V_j^{(s)} - \sum_{m=1}^{s} \binom{s}{m} \times \left(\sum_{k=1}^{N} Z_{jk}^{(m)} I_k^{(s-m)} \right) \right],\ s = 0, 1, \ldots, t \tag{24}$$

where $I_i^{(s)}$ is the s^{th} derivative with respect to k of the i^{th} element of $\vec{I}$ and Y_{ij} is the ij^{th} element of Z^{-1}. The summation with respect to m in (24) is to be omitted when $s = 0$. The summation index k in (24) is not to be confused with $k = \omega\sqrt{\mu\epsilon}$. Note that the derivatives of the moment matrix and the excitation vector have to be expressed analytically before their numerical computation.

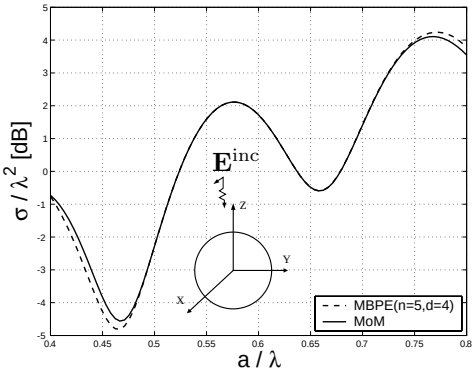

Fig. 1. Normalized RCS of a conducting sphere of radius a using MBPE ($n = 5$ and $d = 4$) and the MoM solution from $a/\lambda = 0.4$ to $a/\lambda = 0.8$. The sampling point of MBPE is at $a/\lambda = 0.6$.

III. Numerical results

The results of applying MBPE to BOR using MoM are considered below. RCS calculations over frequency bands are done for a conducting sphere, a conducting spherical shell with a 5 degree hole and another with a 30 degree hole, a conducting finite circular cylinder of radius a and height $h(= 2a)$ with flat end faces, a conducting cone-sphere structure, and a conducting cylindrical container. The excitation is a plane wave axially incident. The numerical data obtained using MBPE are compared with the results calculated using the pointwise approach. All the computations reported below were done with a Pentium IV 2.0 Ghz computer.

Triangle and pulse basis functions are put on the generating curve of the conducting sphere in Figures 1 and 2 resulting in 61 unknown current coefficients.

Figure 1 shows two normalized RCS's, MoM and MBPE ($n = 5$ and $d = 4$). The MoM RCS is calculated by MoM at 100 equally spaced points from $a/\lambda = 0.4$ to $a/\lambda = 0.8$. The MBPE RCS is obtained by using information only at $a/\lambda = 0.6$. The MoM solutions for the RCS at the 100 points took 117 seconds of CPU time. On the other hand, the MBPE took 14 seconds of CPU time to obtain the RCS at the same points. The MBPE result agrees with the MoM result to within 1% error between $a/\lambda = 0.49$ and $a/\lambda = 0.73$. MBPE achieves 88% reduction compared to the MoM solution where the % reduction is defined by

$$\%\,\text{reduction} = \frac{\text{MoM} - \text{MBPE}}{\text{MoM}} \times 100. \tag{25}$$

In Figure 2 both MBPE's use $n = 5$ and $d = 4$ in (22). The one-frequency MBPE in Figure 2 uses (22) and the first nine derivatives of (22). The two-frequency MBPE in Figure 2 uses (22) at both $a/\lambda = 0.5$ and $a/\lambda = 0.7$, the first four derivatives of (22) at $a/\lambda = 0.5$, and the first four derivatives of (22) at $a/\lambda = 0.7$. The one-frequency MBPE took 14 seconds of CPU time to compute the RCS at 100 equally spaced frequencies whereas the two-frequency MBPE took 27 seconds of CPU time to compute the RCS at the same 100 frequencies. The MoM solution, however, took 117 seconds. The one-frequency MBPE achieves 88% reduction whereas the two-frequency MBPE does 77% reduction. The former agrees with

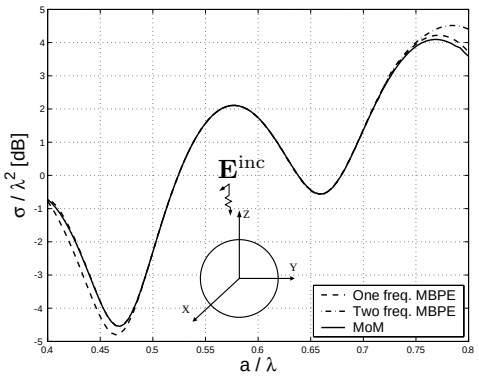

Fig. 2. Normalized RCS of a conducting sphere of radius a using the MoM solution, the one-frequency MBPE, and the two-frequency MBPE from $a/\lambda = 0.4$ to $a/\lambda = 0.8$. The sampling point of the one-frequency MBPE is at $a/\lambda = 0.6$ and the sampling points of the two-frequency MBPE are at $a/\lambda = 0.5$ and $a/\lambda = 0.7$.

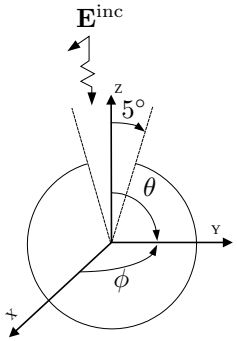

Fig. 3. Geometry of a conducting spherical shell of radius a with a 5 degree hole.

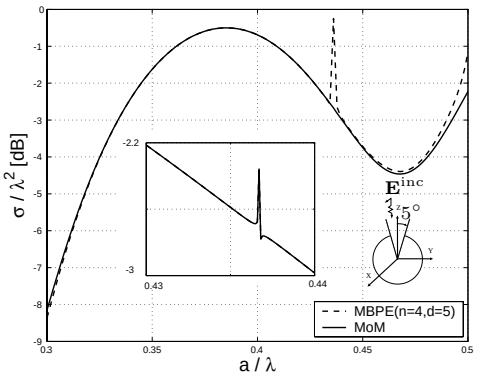

Fig. 4. Normalized RCS of a conducting spherical shell of radius a with a 5 degree hole using MBPE ($n = 4, d = 5$) and the MoM solution from $a/\lambda = 0.3$ to 0.5. The sampling point is at $a/\lambda = 0.4$.

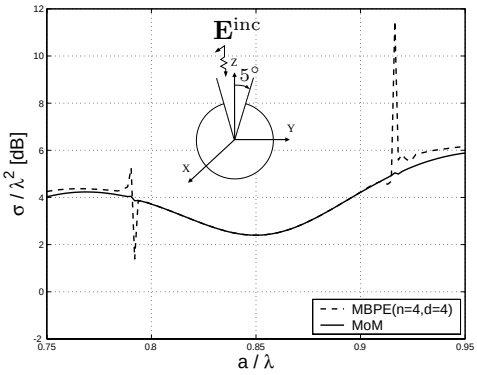

Fig. 5. Normalized RCS of a conducting spherical shell of radius a with a 5 degree hole using MBPE ($n = 4, d = 4$) and the MoM solution from $a/\lambda = 0.75$ to $a/\lambda = 0.95$. The sampling point is at $a/\lambda = 0.85$.

the MoM result to within 1% error between $a/\lambda = 0.49$ to $a/\lambda = 0.73$. On the other hand, the latter agrees with the MoM result to within 1% error between $a/\lambda = 0.43$ to $a/\lambda = 0.72$. In terms of the computational time, the former is less than the latter, but the latter shows better agreement at the low end of the frequency range.

For the demonstration purpose of indicating extremely sharp resonances, a conducting spherical shell of radius a with a 5 degree hole is considered in Figure 3.

In Figure 4, triangle and pulse basis functions are put on the generating curve of the spherical shell resulting in 61 unknown current coefficients. The RCS is calculated at 120 equally spaced points from $a/\lambda = 0.3$ to $a/\lambda = 0.5$. Figure 4 shows the normalized RCS in the vicinity of an extremely sharp resonance and the MBPE sampling point is at $a/\lambda = 0.4$. The MBPE indicates the extremely sharp resonance efficiently whereas MoM does not. MoM took 135 seconds of CPU time to compute the RCS at the 120 points. On the other hand, MBPE took only 15 seconds of CPU time to compute the RCS at the 120 points. As insinuated earlier, the conventional method requires an excessive number of closely spaced samples to obtain the extremely sharp resonance. In this example, although we took 120 equally spaced sampling points, MoM fails to indicate the extremely sharp resonance. An insert in Figure 4 shows MoM clearly indicates the extremely sharp resonance when 201 equally spaced points from $a/\lambda = 0.43$ to $a/\lambda = 0.44$ are taken.

Figure 5 shows the normalized RCS in the vicinity of two extremely sharp resonances. The MBPE sampling point is at $a/\lambda = 0.85$. Triangle and pulse basis functions are put on the generating curve of the spherical shell resulting in 81 unknown current coefficients. The RCS is calculated at 120 equally spaced points from $a/\lambda = 0.75$ to $a/\lambda = 0.95$. The MBPE indicates two extremely sharp resonances at around $a/\lambda = 0.79$ and $a/\lambda = 0.92$. The MBPE curve adequately indicates the extremely sharp resonances and agrees to within 1% error between the extremely sharp resonances, but elsewhere it deviates from the MoM curve. MBPE took 26 seconds of CPU time to compute the RCS at the 120 points whereas MoM took 242 seconds of CPU time to compute the RCS at the same points, that is, MBPE obtains 89% reduction.

Figure 6 shows the geometry of a spherical shell of radius a with a 30 degree hole.

Figure 7 shows the normalized RCS using the one-frequency MBPE, the two-frequency MBPE, and MoM. Triangle and pulse basis functions are put on the generating curve of the spherical shell resulting in 41 unknown current coefficients. The RCS curves are calculated at 91 equally spaced points from $a/\lambda = 0.1$ to $a/\lambda = 0.4$. Both MBPE's use $n = 5$ and $d = 4$ in (22). The sampling point of the one-frequency MBPE is at $a/\lambda = 0.25$ and the sampling points of the two-frequency

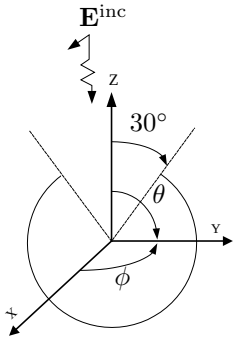

Fig. 6. Geometry of a conducting spherical shell of radius a with a 30 degree hole.

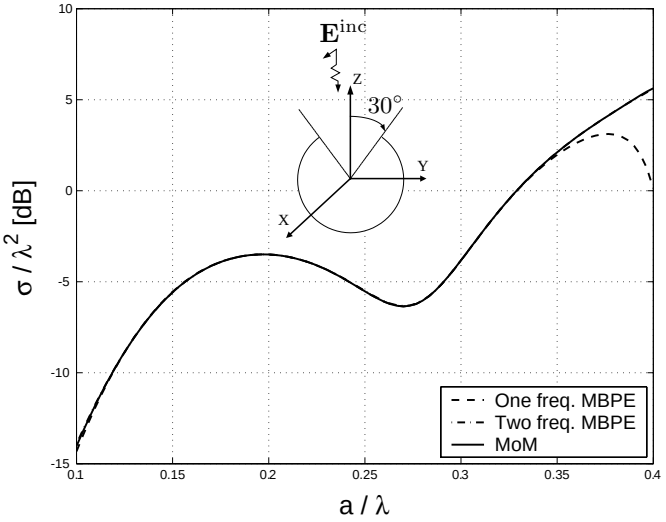

Fig. 7. Normalized RCS of a conducting spherical shell of radius a with a 30 degree hole using the one-frequency MBPE, the two-frequency MBPE, and MoM from $a/\lambda = 0.1$ to $a/\lambda = 0.4$. The sampling point of the one-frequency MBPE is at $a/\lambda = 0.25$ and the sampling points of the two-frequency MBPE are at $a/\lambda = 0.17$ and $a/\lambda = 0.35$.

MBPE are at $a/\lambda = 0.17$ and $a/\lambda = 0.35$. The one-frequency MBPE took 8 seconds of CPU time (83% reduction) and the two-frequency MBPE took 14 seconds of CPU time (70% reduction), whereas MoM took 47 seconds of CPU time. The two-frequency MBPE curve shows better agreement between $a/\lambda = 0.1$ and $a/\lambda = 0.4$ than the one-frequency MBPE curve.

Figure 8 shows the normalized RCS using the one-frequency MBPE, the two-frequency MBPE, and MoM. Triangle and pulse basis functions are put on the generating curve of the spherical shell resulting in 81 unknown current coefficients. The RCS curves are calculated at 121 equally spaced points from $a/\lambda = 0.35$ to $a/\lambda = 0.65$. Both MBPE's use $n = 4$ and $d = 5$ in (22). The sampling point of the one-frequency MBPE is at $a/\lambda = 0.5$ and the sampling points of the two-frequency MBPE are at $a/\lambda = 0.44$ and $a/\lambda = 0.59$. The one-frequency MBPE took 25 seconds of CPU time (89% reduction) and the two-frequency MBPE took 46 seconds of CPU time (80% reduction), whereas MoM took 229 seconds of CPU time. It can be seen that the two-frequency MBPE curve agrees with MoM to within 1% error between $a/\lambda = 0.39$ and $a/\lambda = 0.64$, whereas the one-frequency MBPE curve agrees with MoM to within 1% error only between $a/\lambda = 0.44$ and $a/\lambda = 0.57$.

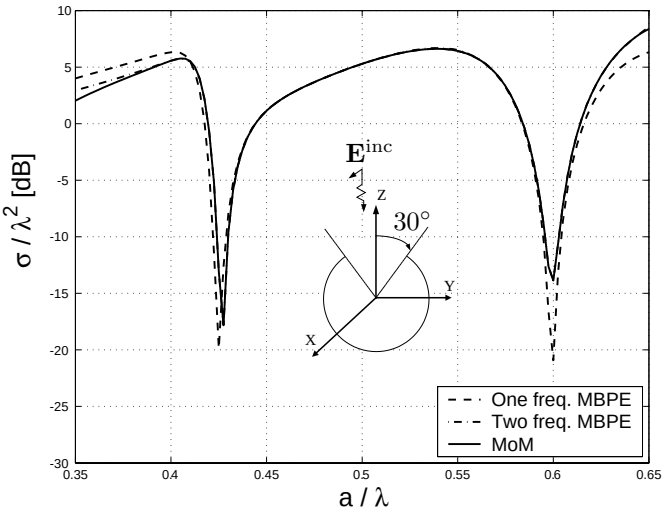

Fig. 8. Normalized RCS of a conducting spherical shell of radius a with a 30 degree hole using the one-frequency MBPE, the two-frequency MBPE, and MoM from $a/\lambda = 0.35$ to $a/\lambda = 0.65$. The sampling point of the one-frequency MBPE is at $a/\lambda = 0.5$ and the sampling points of the two-frequency MBPE are at $a/\lambda = 0.44$ and $a/\lambda = 0.59$.

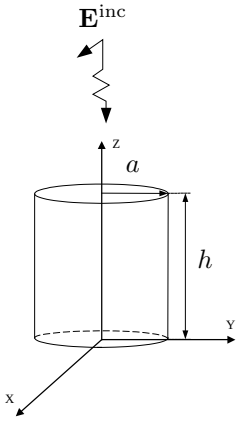

Fig. 9. Geometry of a conducting finite circular cylinder of radius a and height h with flat end faces.

Figure 9 shows the geometry of a conducting finite circular cylinder of radius a and height h.

Figure 10 shows the normalized RCS of a conducting finite circular cylinder of radius a and height $2a$ with flat end faces using the one-frequency MBPE, the two-frequency MBPE, and MoM. Triangle and pulse basis functions are put on the generating curve of the cylinder resulting in 81 unknown current coefficients. The RCS curves are calculated at 100 equally spaced points from $a/\lambda = 0.02$ to $a/\lambda = 0.4$. Both MBPE's use $n = 5$ and $d = 4$ in (22). The sampling point of the one-frequency MBPE is at $a/\lambda = 0.2$ and the sampling points of the two-frequency MBPE are at $a/\lambda = 0.1$ and $a/\lambda = 0.29$. The one-frequency MBPE took 25 seconds of CPU time (87% reduction) and the two-frequency MBPE took 46 seconds of CPU time (76% reduction), whereas MoM took 191 seconds of CPU time. The two-frequency MBPE curve shows slightly better agreement than the one-frequency MBPE curve especially around $a/\lambda = 0.02$.

Figure 11 shows the normalized RCS of the conducting finite circular cylinder of radius a and height $2a$ with flat end faces

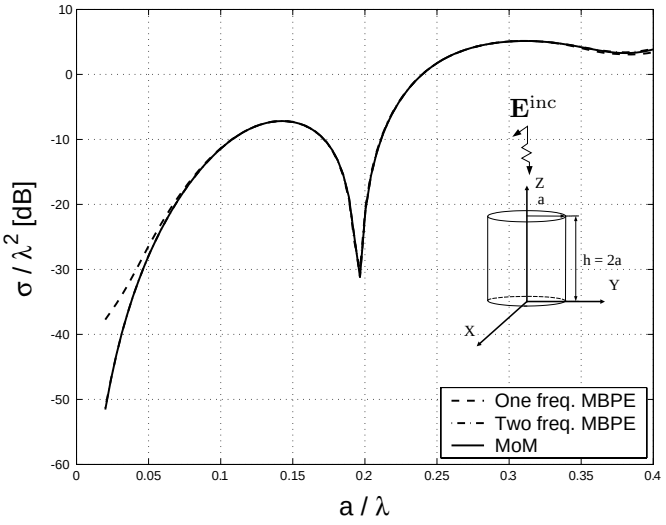

Fig. 10. Normalized RCS of a conducting finite circular cylinder of radius a and height $2a$ with flat end faces from $a/\lambda = 0.02$ to $a/\lambda = 0.4$. The sampling point of the one-frequency MBPE is at $a/\lambda = 0.2$ and the sampling points of the two-frequency MBPE are at $a/\lambda = 0.1$ and $a/\lambda = 0.29$.

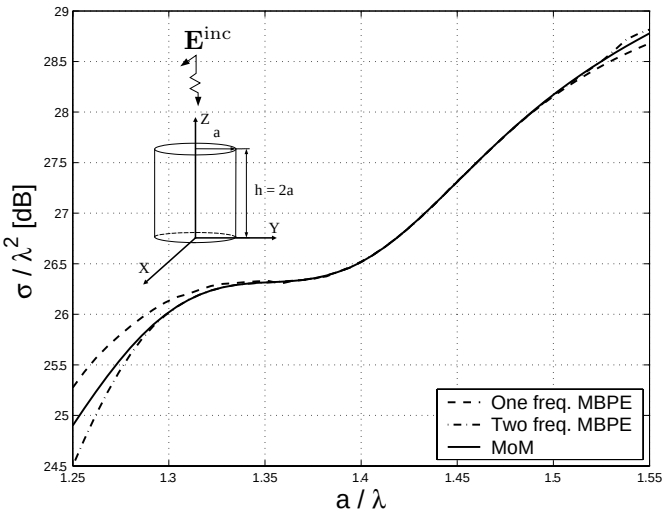

Fig. 11. Normalized RCS of the conducting finite circular cylinder of radius a and height $2a$ with flat end faces from $a/\lambda = 1.25$ to $a/\lambda = 1.55$. The sampling point of the one-frequency MBPE is at $a/\lambda = 1.4$ and the sampling points of the two-frequency MBPE are at $a/\lambda = 1.32$ and $a/\lambda = 1.46$.

in a higher frequency band using the one-frequency MBPE, the two-frequency MBPE, and MoM. Triangle and pulse basis functions are put on the generating curve of the cylinder resulting in 201 unknown current coefficients. The RCS curves are calculated at 100 equally spaced points from $a/\lambda = 1.25$ to $a/\lambda = 1.55$. Both MBPE's use $n = 5$ and $d = 4$ in (22). The sampling point of the one-frequency MBPE is at $a/\lambda = 1.4$ and the sampling points of the two-frequency MBPE are at $a/\lambda = 1.32$ and $a/\lambda = 1.46$. The one-frequency MBPE took 153 seconds of CPU time (88% reduction) and the two-frequency MBPE took 291 seconds of CPU time (77% reduction), whereas MoM took 1289 seconds of CPU time. The two-frequency MBPE curve shows slightly better agreement between $a/\lambda = 1.25$ and $a/\lambda = 1.55$ than the one-frequency MBPE curve.

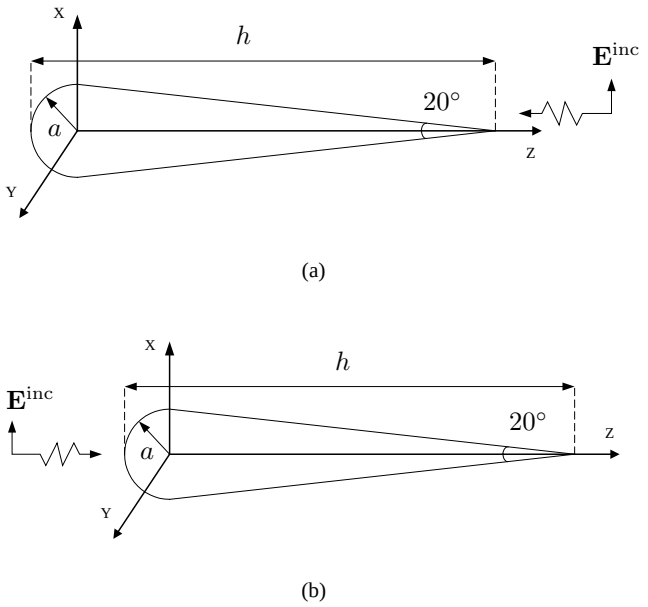

Fig. 12. Geometry of a cone-sphere structure illuminated by a plane wave which is axially incident and propagates either (a) from the cone tip toward the spherical cap or (b) from the spherical cap toward the cone tip.

Figure 12 shows the geometry of a cone-sphere structure illuminated by a plane wave which is axially incident and propagates either from the cone tip toward the spherical cap or from the spherical cap toward the cone tip.

Figure 13 shows the normalized RCS of the cone-sphere in Figure 12(a) using the one-frequency MBPE, the two-frequency MBPE, and MoM. The incident wave propagates from the cone tip toward the spherical cap. Triangle and pulse basis functions are put on the generating curve of the cone-sphere resulting in 61 unknown current coefficients. The RCS curves are calculated at 100 equally spaced points from $a/\lambda = 0.02$ to $a/\lambda = 0.4$. Both MBPE's use $n = 5$ and $d = 4$ in (22). The sampling point of the one-frequency MBPE is at $a/\lambda = 0.2$ and the sampling points of the two-frequency MBPE are at $a/\lambda = 0.14$ and $a/\lambda = 0.26$. The one-frequency MBPE took 14 seconds of CPU time (89% reduction) and the two-frequency MBPE took 26 seconds of CPU time (79% reduction), whereas MoM took 124 seconds of CPU time. The two-frequency MBPE curve agrees with MoM to within 1% error between $a/\lambda = 0.08$ and $a/\lambda = 0.32$, whereas the one-frequency MBPE curve agrees with MoM to within 1% error between $a/\lambda = 0.16$ and $a/\lambda = 0.24$.

Figure 14 shows the normalized RCS of the cone-sphere structure in Figure 12(b) using the one-frequency MBPE, the two-frequency MBPE, and MoM. The incident wave propagates from the spherical cap toward the cone tip. Triangle and pulse basis functions are put on the generating curve of the cone-sphere resulting in 61 unknown current coefficients. The RCS curves are calculated at 100 equally spaced points from $a/\lambda = 0.02$ to $a/\lambda = 0.4$. Both MBPE's use $n = 5$ and $d = 4$ in (22). The sampling point of the one-frequency MBPE is at $a/\lambda = 0.2$ and the sampling points of the two-frequency MBPE are at $a/\lambda = 0.14$ and $a/\lambda = 0.26$. The one-frequency

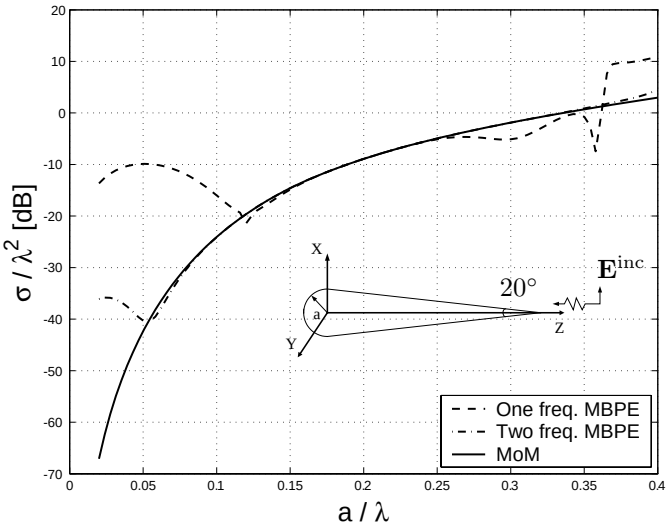

Fig. 13. Normalized RCS of a cone-sphere structure illuminated by a plane wave which is axially incident and propagates from the cone tip toward the spherical cap between $a/\lambda = 0.02$ and $a/\lambda = 0.4$. The sampling point of the one-frequency MBPE is at $a/\lambda = 0.2$ and the sampling points of the two-frequency MBPE are at $a/\lambda = 0.14$ and $a/\lambda = 0.26$.

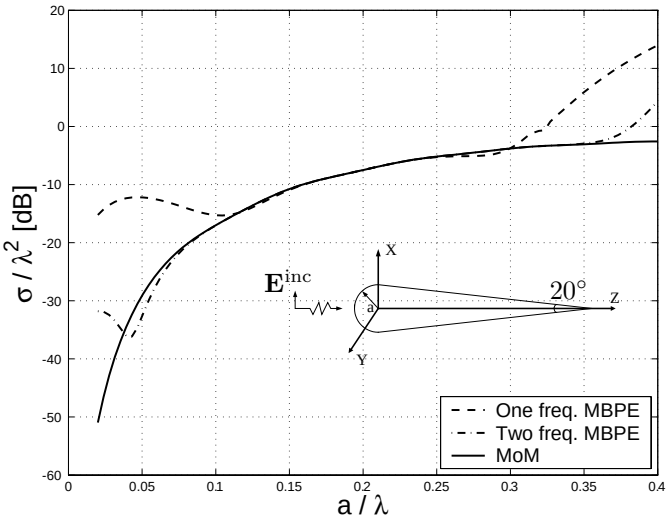

Fig. 14. Normalized RCS of a cone-sphere structure illuminated by a plane wave which is axially incident and propagates from the spherical cap toward the cone tip between $a/\lambda = 0.02$ and $a/\lambda = 0.4$. The sampling point of the one-frequency MBPE is at $a/\lambda = 0.2$ and the sampling points of the two-frequency MBPE are at $a/\lambda = 0.14$ and $a/\lambda = 0.26$.

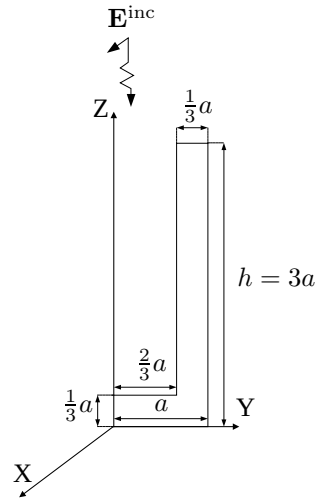

Fig. 15. Geometry of a conducting cylindrical container of outside diameter a, inside diameter $\frac{2}{3}a$, height $3a$, and thickness $\frac{1}{3}a$.

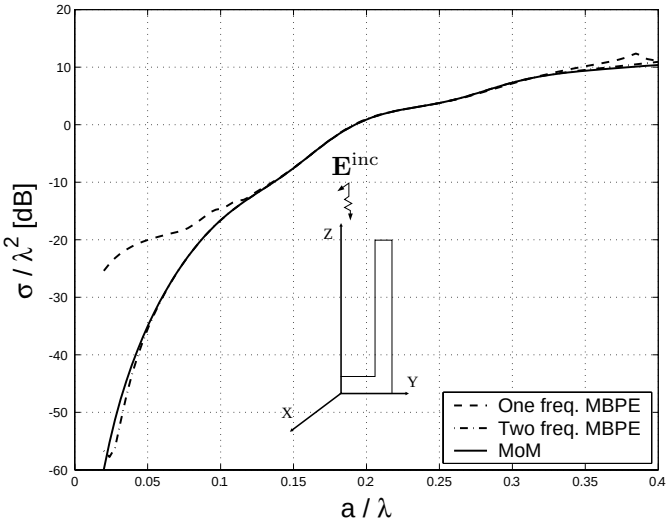

Fig. 16. Normalized RCS of a conducting cylindrical container from $a/\lambda = 0.02$ to $a/\lambda = 0.4$. The sampling point of the one-frequency MBPE is at $a/\lambda = 0.2$ and the sampling points of the two-frequency MBPE are at $a/\lambda = 0.12$ and $a/\lambda = 0.28$.

MBPE took 14 seconds of CPU time (89% reduction) and the two-frequency MBPE took 26 seconds of CPU time (79% reduction), whereas MoM took 124 seconds of CPU time. The two-frequency MBPE curve agrees with MoM to within 1% error between $a/\lambda = 0.08$ and $a/\lambda = 0.34$, whereas the one-frequency MBPE curve agrees with MoM to within 1% error between $a/\lambda = 0.15$ and $a/\lambda = 0.24$.

Figure 15 shows the geometry of a conducting cylindrical container of outside diameter a, inside diameter $\frac{2}{3}a$, height $3a$, and thickness $\frac{1}{3}a$.

Figure 16 shows the normalized RCS of the conducting cylindrical container by using the one-frequency MBPE, the two-frequency MBPE, and MoM. Triangle and pulse basis functions are put on the generating curve of the container resulting in 93 unknown current coefficients. The RCS curves are calculated at 100 equally spaced points from $a/\lambda = 0.02$ to $a/\lambda = 0.4$. Both MBPE's use $n = 5$ and $d = 4$ in (22). The sampling point of the one-frequency MBPE is at $a/\lambda = 0.2$ and the sampling points of the two-frequency MBPE are at $a/\lambda = 0.12$ and $a/\lambda = 0.28$. The one-frequency MBPE took 34 seconds of CPU time (88% reduction) and the two-frequency MBPE took 63 seconds of CPU time (78% reduction), whereas MoM took 289 seconds of CPU time. The two-frequency MBPE curve agrees with MoM to within 1% error between $a/\lambda = 0.05$ and $a/\lambda = 0.35$, whereas the one-frequency MBPE curve agrees with MoM to within 1% error between $a/\lambda = 0.14$ and $a/\lambda = 0.26$.

IV. CONCLUSIONS

An implementation of MBPE for the BOR using MoM in the frequency domain is presented. The RCS for various PEC objects such as a sphere, a spherical shell with a 5 degree hole or with a 30 degree hole, a finite cylinder with flat end faces, a cone-sphere structure, and a conducting cylindrical container are computed and compared with the MoM solutions over frequency bands. Instead of using a pointwise approach, a rational function model is used to approximate the induced surface as a function of frequency. The model coefficients are computed using frequency and frequency-derivative information at one frequency in the band or alternatively at two frequencies in the band. Sample results show the MBPE approach gives excellent results over a limited frequency band, and is much more efficient than the conventional pointwise approach.

As seen in numerical results, the two-frequency MBPE gives better agreement than the one-frequency MBPE in terms of accuracy although a rational function of the same order is used. But the former requires adjustment at two sampling points to obtain the best results, whereas the latter does not.

Even though a higher order model generally gives a better approximation, careful treatment of the model is required. For instance, high order ($n + d \geq 7$) derivatives in the one-frequency MBPE make the sampling matrices ill-conditioned. To avoid this problem, use of the two-frequency MBPE with the same order model is recommended.

Note that the E-field solution fails to provide a unique solution for the current on a conducting body at any resonant frequency of the region enclosed by the conducting surface of the body. Thus, if a sampling point of the MBPE is accidently at or in the vicinity of a resonant frequency, the results would not be reliable. This problem is more likely to occur when the MBPE is applied to an electrically very large body. Because an electrically large body has resonant frequencies that are close together, wherever a sampling point is chosen it is likely to be in the vicinity of an internal resonant frequency. The problem can be avoided by using the combined field solution instead of the E-field solution. The combined field solution uses a linear combination of the E-field and H-field integral equations. When the combined field solution is used, the MBPE will not incur loss of accuracy caused by proximity to an internal resonant frequency.

REFERENCES

[1] G. J. Burke and E. K. Miller, "Use of frequency-derivative information to reconstruct an electromagnetic transfer function," *Proceedings of the fourth annual ACES review,* Naval Postgraduate School, Monterey, CA, Mar. 1988.

[2] G. J. Burke, E. K. Miller, S. Chakrabarti, and K. Demarest, "Using model-based parameter estimation to increase the efficiency of computing electromagnetic transfer functions," *IEEE Trans. Magnetics*, vol. 25, no. 4, pp. 2807–2809, July 1989.

[3] K. R. Demarest, E. K. Miller, K. Kalbasi, and L. K. Wu, "A computationally efficient method of evaluating Green's functions for 1-, 2-, and 3-D enclosures," *IEEE Trans. Magnetics*, vol. 25, no. 4, pp. 2878–2880, July 1989.

[4] X. Yang and E. Arvas, "Resonance region scattering," Final technical report, RADC-TR-90-1, Rome Air Development Center, Griffiss Air Force base, NY 13441, USA, Mar. 1990.

[5] X. Yang and E. Arvas, "Use of frequency-derivative information in two-dimensional electromagnetic scattering problems," *Proc. Inst. Elect. Eng.*, pt. H, vol. 138, no. 4, pp. 269–272, Aug. 1991.

[6] C. J. Reddy, M. D. Deshpande, C. R. Cockrell, and F. B. Beck, "Fast RCS computation over a frequency band using method of moments in conjunction with asymptotic waveform evaluation technique," *IEEE Trans. Antennas Propagat.*, vol. 46, no. 8, pp. 1229–1233, Aug. 1998.

[7] C. J. Reddy, "Application of model based parameter estimation for RCS frequency response calculations using method of moments," Contractor Report, NASA/CR-1998-206951, Hampton University, Hampton, VA 23668, Mar. 1998.

[8] K. Kottapalli, T. K. Sarkar, Y. Hua, E. K. Miller, and G. J. Burke, "Accurate computation of wide-band response of electromagnetic systems utilizing narrow-band information," *IEEE Trans. Microwave Theory Tech.*, vol. 39, no. 4, pp. 682–687, Apr. 1991.

[9] M. G. Andreasen, "Scattering from bodies of revolution," *IEEE Trans. Antennas Propagat.*, vol. AP-13, pp. 303–310, Mar. 1965.

[10] J. R. Mautz and R. F. Harrington, "Generalized network parameters for bodies of revolution," Technical Report TR-68-7, Syracuse University, Syracuse, NY 13244, June 1968.

[11] J. R. Mautz and R. F. Harrington, "Radiation and scattering from bodies of revolution," Appl. Sci. Res., vol. 20, pp. 405–435, June 1969.

[12] J. R. Mautz and R. F. Harrington, "H-field, E-field, and combined field solutions for bodies of revolution," AEÜ, vol. 32, pp. 157–164, Apr. 1978.

[13] J. R. Mautz and R. F. Harrington, "Computer programs for H-field, E-field, and combined field solutions for bodies of revolution," Technical Report, TR-77-3, Syracuse University, Syracuse, NY 13244, May 1977.

[14] J. R. Mautz and R. F. Harrington, "A combined-source solution for radiation and scattering from a perfectly conducting body," *IEEE Trans. Antennas Propagat.*, vol. AP-27, pp. 445–454, July 1979.

[15] A. W. Glisson and D. R. Wilton, "Simple and efficient numerical methods for problems of electromagnetic radiation and scattering from surfaces," *IEEE Trans. Antennas Propagat.*, vol. AP-28, no. 5, pp. 593–603, Sept. 1980.

[16] J. R. Mautz and R. F. Harrington, "An improved E-field solution for a conducting body of revolution," AEÜ, vol. 36, pp. 198–206, May 1982.

Hyunwung Son was born in Busan, Korea, in 1972. He received the B.S. degree in electronics engineering from Kyunghee University, Korea, in 1997 and the M.S. and Ph.D. degrees in electrical engineering from Syracuse University, Syracuse, NY, in 2000 and 2003, respectively.

He is currently a Senior Research Engineer in LG Electronics, Seoul, Korea. His current research interests include numerical electromagnetics, radiation, scattering, antenna design, and microwave circuits and devices.

Joseph. R. Mautz was born in Syracuse, NY, in 1939. He received the B.S., M.S., and Ph.D. degrees in electrical engineering from Syracuse University, Syracuse, NY, in 1961, 1965, and 1969, respectively.

Until July 1993, he was a Research Associate in the Department of Electrical and Computer Engineering of Syracuse University, working on radiation and scattering problems. His primary fields of interest are electromagnetic theory and applied mathematics. He is presently an adjacent professor in the Department of Electrical Engineering and Computer Science, Syracuse University.

Ercument Arvas received the B.S. and M.S. degrees from METU, Ankara, Turkey, in 1976 and 1979, respectively, and the Ph.D. degree from Syracuse University, Syracuse, NY, in 1983, all in electrical engineering.

From 1984 to 1987, he was with the Electrical Engineering Department, Rochester Institute of Technology, Rochester, NY. He joined the Department of Electrical Engineering and Computer Science, Syracuse University, in 1987, where he is currently a Professor. His research interests include numerical electromagnetics, antennas, and microwave circuits and devices.